

Research Article

## An Evidence of Drug Repurposing for COVID-19 Pandemic Based on *In silico* Investigation from Phenolic Derivatives of Silybum Marianum Against SARS-Cov-2 Proteins

Swaraj Mohanty <sup>1</sup>, Soumya Lipsa Rath <sup>2</sup>, Poornima Sharma <sup>1</sup>, Yasmin Ahmad <sup>1,\*</sup>

1. Pathophysiology and Disruptive Technology (PDT) Division, Defence Institute of Physiology & Allied Sciences (DIPAS), Defence Research & Development Organization (DRDO), Lucknow Road, Timarpur, Delhi-110054, India; E-Mails: [yasminchem@gmail.com](mailto:yasminchem@gmail.com); [mohanty.swaraj2@gmail.com](mailto:mohanty.swaraj2@gmail.com); [poornimasharmajan366@gmail.com](mailto:poornimasharmajan366@gmail.com)
2. Department of Biotechnology, National Institute of Technology (NIT), Warangal, Telengana-506004, India; E-Mail: [slrath@nitw.ac.in](mailto:slrath@nitw.ac.in)

\* **Correspondence:** Yasmin Ahmad; E-Mail: [yasminchem@gmail.com](mailto:yasminchem@gmail.com)**Academic Editor:** Xiangzi Han**Special Issue:** [Oxygen Transport Physiology and COVID at High Altitude](#)*OBM Genetics*

2023, volume 7, issue 3

doi:10.21926/obm.genet.2303186

**Received:** January 11, 2023**Accepted:** June 19, 2023**Published:** July 04, 2023

### Abstract

The outbreak of coronavirus disease-2019 (COVID-19) had a striking impact on the worldwide healthcare system within a very short period. The availability of a large number of clinical data on SARS-CoV-2, conventional precautionary majors, and treatment strategies with the existing therapeutic antiviral drug molecules also fails to control progression and disease transmission among the population. Hence, we implemented pharmacoinformatics approaches to facilitate the drug discovery by repurposing naturally available therapeutic molecules as an effective intervention. The major phenolic derivatives of *Silybum marianum* (Milk thistle) have been identified and investigated for ADME (Absorption, Distribution, Metabolism and Excretion)/tox properties. Co-crystallized structure of three major proteins (i.e., main protease, RNA binding domain of nucleocapsid phosphoprotein and Spike receptor binding domain) from SARS-CoV-2 investigated with molecular docking (MD) interaction with the



© 2023 by the author. This is an open access article distributed under the conditions of the [Creative Commons by Attribution License](#), which permits unrestricted use, distribution, and reproduction in any medium or format, provided the original work is correctly cited.

phenolic compounds from milk thistle. Furthermore, a 100 ns MD simulation was performed with silibinin molecule based on ADMET and MD interaction. Being less toxic in ADME, a good MD interaction and stability of silibinin molecule across the MD simulation trajectories with targeted proteins explicate that silibinin molecule can be a promising drug candidate against the main protease and will be helpful to cease the enzymatic activity in viral replication and transcription.

### Keywords

SARS-CoV-2; ADMET; molecular docking; silibinin; molecular dynamic (MD) simulations; drug repurposing

## 1. Introduction

In late 2019, the outbreak of COVID-19 completely changed the global healthcare scenario. This highly communicable disease created an emergency healthcare condition across the globe. The countries were also affected during this global pandemic due to poor hospital management conditions and economic crashes. Nevertheless, considering the situation's urgency, companies worldwide worked towards generating vaccines and alternative therapeutics to eradicate the disease globally. However, this objective could not be achieved completely due to the emergence of new variants of the virus and the increasing drug resistance and escape strategies of the virus.

Developing a new drug or a vaccine is tedious, from drug discovery to in-vitro screening, preclinical and clinical trials. Gaining FDA approval requires a minimum of 12 to 15 years, which is too long considering the mortality rate of COVID-19. An alternative strategy that can boost the process is to repurpose existing drugs. Repurposing FDA-approved drugs drastically reduces the time and costs incurred in manufacturing. Major flavonolignans such as silibinin, isosilybin, silychristin and silidianin from *Silybum marianum* are most prominently known for their medicinal properties to cure different disease states of the liver like chronic liver cirrhosis [1], fibrosis [2], necrosis [3, 4] and hepatocellular carcinoma [5, 6]. This compound is also well known for its anti-inflammatory, antioxidant, anti-carcinogenic and anti-mutagenic properties. Silymarin on the rat as an animal model demonstrated that it helps in the prevention of free radical generation of reactive oxygen species (ROS), triggers the antioxidant defense system, improves the anti-inflammatory response and activates the key genes that act as compensatory adaptive vascular response during the hypoxic condition [1, 7]. As silymarin is in the clinical trial pipeline and its less toxic properties is a unique characteristic that can ensure it as an effective drug molecule for a different disease, we evaluated the efficacy of the molecule towards main protease, spike receptor binding domain and RNA binding domain of nucleocapsid phosphoprotein enzymes of SARS-CoV-2 [8]. The COVID-19 disease affects the endothelial lining of the lungs and the disease progression also relates to physiological changes as in the case of high-altitude hypoxia illness [9]. Hence, we want to check the possibility of silibinin (a major constituent of silymarin) as an effective inhibitor.

The SARS-CoV-2 genome consists of 12 open reading frames (ORFs), 9 transcription regulatory sequences, 9 conserved leader sequences and 2 untranslated regions (UTRs) [10] (Figure 1). The multiple sequence alignment data of the SARS-CoV-1 & SARS-CoV-2 shows the sequence similarities,

and it is believed that 10-28 nucleotides in the 5' UTR interacts with the non-structural protein1 (Nsp1). Targeting the major viral protein to stop the progression of pathogenesis needs a clear understanding of the viral genome and its translational units that interact with different host machinery, starting from the viral entry till the hijack of the cell immunity [11]. Among the four structural proteins of the SARS-CoV-2 virus we have targeted the binding sites of major proteins, i.e., the RNA binding domain of the nucleocapsid of phosphoprotein and the receptor binding domain of spike protein. From the virology aspects main proteases play a major role in viral proprotein maturation and assembly of other components to produce a whole virus after the translational event inside the host cell. We also targeted the cysteine-like protease, i.e., the main protease of the ORF1a region [8, 12]. Hence investigation to find the major inhibitory molecule that can actively bind and block the enzymatic activity of the major proteins of SARS-CoV-2 is necessary to break the chain of the disease transmission from the pharmacological point of cure.

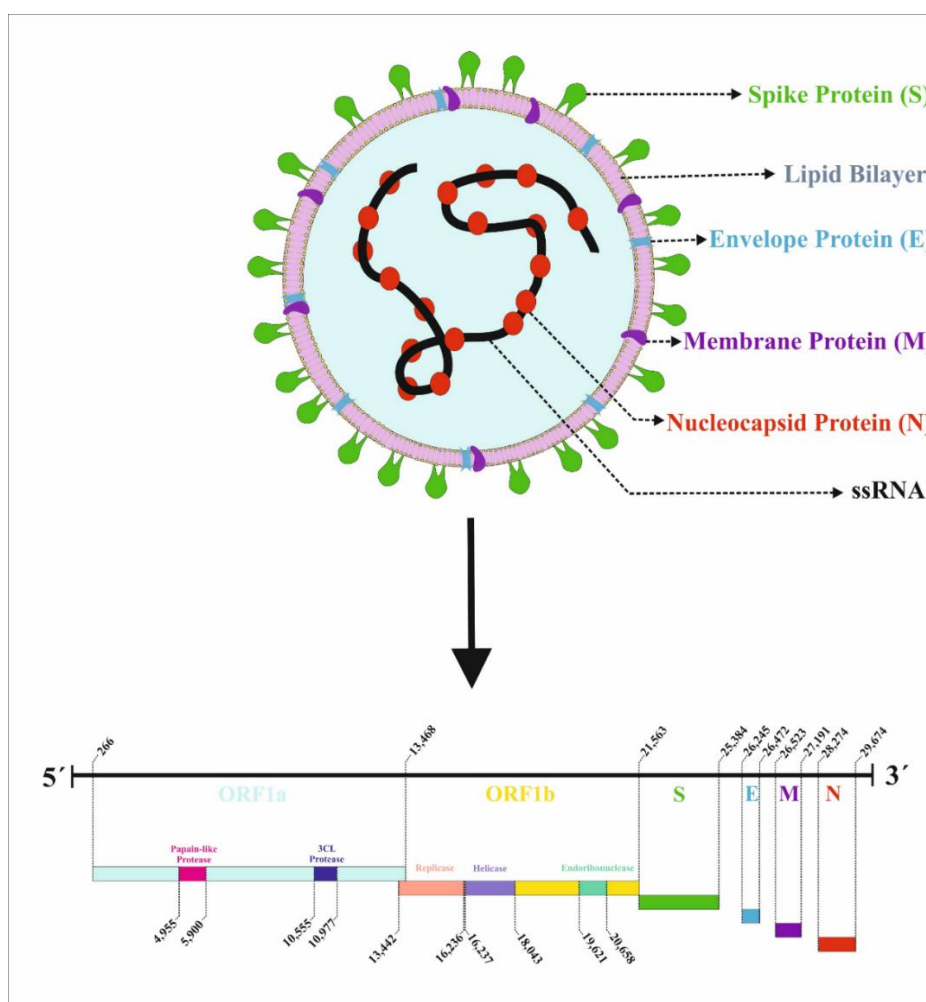


**Figure 1** The genome organization of SARS-CoV-2 and its translational regions.

## 2. Materials and Methods

### 2.1 Molecular Docking and ADME/Tox Analysis

The 3D structural data files (SDFs) of ligands (CID: 31553, 3085830, 441764 & 1982272) of *Silybum marianum* were taken from the PubChem database (<https://pubchem.ncbi.nlm.nih.gov/>)

and checked for the pharmacokinetics and toxicity properties with ADMELab 2.0 (<https://admetmesh.scbdd.com/>). This ADMELab 2.0 tool is considered to efficiently calculate and predict 17 physiochemical, 13 medicinal chemistry properties, 23 different ADME, and 27 toxicity endpoints along with the 8 toxicophore rules.

The crystallographic structures of the proteins of SARS-CoV-2 were imported from the protein data bank (PDB ID: 6LU7, 6VYO & 7BZ5). The ligands were transformed into PDBQT file format by using Open Babel (Version 3.1.1) tool [13]. The refinement of protein structures was done with AutoDock Vina (version 1.2.0) tool developed at The Scripps Research Institute [14]. The protein structures were imported, and the water molecules present in the crystal structure data were removed. Interacting small molecules were also removed from the structure, and missing residues and polar hydrogen molecules were appended. The refined structures were subjected to energy minimization and then a grid box with a dimension of X, Y & Z coordinates = 126.0 and spacing 0.375 Ang was used for blind docking. The center of the grid was fixed as: -center\_x = -26.286, center\_y = 12.608 & center\_z = 58.965 for 6LU7, center\_x = -14.253, center\_y = 41.224 & center\_z = 14.164 for 6VYO and center\_x = -72.527, center\_y = -29.929 & center\_z = 11.449 for 7BZ5. Gasteiger charges were added to the protein before docking. All rotatable bonds of ligands were kept flexible while the protein remained rigid during the docking.

## **2.2 Molecular Dynamics Simulation**

Based on the strong docking interaction profile and the lesser toxicity for the silibinin compound in the ADMET results, we focused on studying the molecular evolution and the conformational changes of macromolecules (PDB ID: 6LU7, 6VYO & 7BZ5) with the ligand molecule during the 100 ns molecular dynamics simulation. Molecular Dynamics (MD) Simulation was performed by using GROMACS (version 2020.4) MD simulation software package [15, 16]. Charmm36-jul2020 force field parameters for protein were used for the study [17, 18]. The topology and parameters for ligand molecules were generated using the CHARMM General Force Field Server [19]. The complexes were placed inside a box filled with TIP3P water molecules and neutralizing ions. The box edge was kept at 1 nm from the protein-ligand complex to avoid calculation artifacts. Initial minimization was performed using steepest descent and conjugate gradient algorithms followed by equilibration at an isothermal-isobaric ensemble. A time step of 2 fs was considered during the simulation and A trajectory of 100 ns was generated to obtain data for analysis. Pymol [20, 21] and BIOVIA Discovery studio visualizer [22] were used to analyze structures generated during the study.

## **3. Results and Discussions**

### **3.1 Description of Silibinin & Its Derivatives**

#### **3.1.1 ADME/Tox Properties**

The absorption of any oral drug molecule takes place in the intestinal cells before releasing into the systematic circulation with an active and passive diffusion process. Hence different in vitro models have been developed for the permeability study and oral bioavailability. Likewise, the distribution of the drug after administration has also been calculated along with the concentration-to-volume ratio, plasma protein binding, and the side effect in the central nervous system (CNS).

The metabolism of any drug molecule occurs in the liver using oxidative reaction and conjugative reaction; isozymes of the cytochrome P450 family have been studied. Clearance of the drug molecule, its half-life and toxicity are also crucial parameter in understanding the pharmacokinetic of drug [23]. The four compounds show good medicinal properties as they satisfy the Lipinski rule, Pfizer rule and Golden triangle rule with the silibinin and isosilybin showing medium apparent permeability coefficient( $P_{app}$ ) to estimate the effect of blood-brain barrier(BBB) by considering the Maidin-Darby Canine Kidney cells(MDCK) as an in vitro model. With a moderate P-glycoprotein(P-gp) inhibitor property and excellent P-glycoprotein substrate forming ability of Silibinin and isosilybin is known to protect the body as it maintains the removal of drugs from the kidneys and liver and maintains the integrity of BBB. The metabolism of the intake drug plays a major role in keeping the homeostasis of major organelle of an individual with complex physiological interaction; the very minimal(<1) values of CYP34A substrate and inhibitors from this drug profiling explicitly cite that these are the major molecule accounts for 30-50% of drug metabolites. Silibinin & isosilybin shows a very lower dose intake as per the mmol/kg- bw/day as per the calculation by Food and Drug Administration maximum daily dose(FDAMDD) and lower rat oral acute toxicity which supports these two isoforms to be with an excellent  $F_{20\%}$  oral bioavailability. With a higher acceptance to the Toxicology in the 21<sup>st</sup> century(Tox21) methodology by database screening and excellent scoring of nuclear androgen receptor(NR-AR), NR-AR binding to ligand(NR-AR-LBD), nuclear estrogen receptor(NR-ER) and NR-ER ligand binding affinity these two molecules needs further attention to the pharmacokinetics studies. The effect of the chemical molecules can be well understood from the values (Table 1) and the explanation of different properties are supplied as a supplementary datasheet (Supplementary datasheet).

**Table 1** ADMET Property of Ligands.

<b>Properties</b>	<b>Measuring Properties</b>	<b>Values for Silibinin (31553)</b>	<b>Values for Isosilybin (3085830)</b>	<b>Values for Silychrystin (441764)</b>	<b>Values for Silidianin (11982272)</b>
<b>Absorption</b>	Caco-2 Permeability	-6.255	-6.255	-6.254	-5.155
	MDCK Permeability	$9 \times 10^{-6}$	$9 \times 10^{-6}$	$5 \times 10^{-6}$	$6 \times 10^{-6}$
	Pgp-inhibitor	0.44	0.44	0.02	0.051
	Pgp-substrate	0.002	0.002	0.001	0.023
	HIA	0.366	0.366	0.417	0.708
	F <sub>20%</sub>	0.005	0.005	0.013	0.099
	F <sub>30%</sub>	0.846	0.846	0.978	0.866
<b>Distribution</b>	Plasma Protein Binding (PPB)	96.65%	96.65%	95.27%	95.81%
	Volume Distribution (VD)	0.649	0.649	0.6	0.563
	Blood Brain Barrier (BBB) Penetration	0.024	0.024	0.021	0.002
	Fraction Unbound (Fu) in plasms	5.733%	5.733%	6.404%	3.151%
	<b>Metabolism</b>	CYP1A2 inhibitor	0.038	0.038	0.041
CYP1A2 substrate		0.106	0.106	0.137	0.935
CYP2C19 inhibitor		0.12	0.12	0.037	0.044
CYP2C19 substrate		0.067	0.067	0.061	0.216
CYP2C9 inhibitor		0.664	0.664	0.504	0.451
CYP2C9 substrate		0.828	0.828	0.718	0.82
CYP2D6 inhibitor		0.31	0.31	0.091	0.074
CYP2D6 substrate		0.419	0.419	0.225	0.216
CYP3A4 inhibitor		0.785	0.785	0.614	0.374
CYP3A4 substrate		0.343	0.343	0.353	0.723
<b>Excretion</b>	Clearance (CL)	5.144	5.144	6.617	9.112
	Half Life (T <sub>1/2</sub> )	0.274	0.274	0.409	0.558

<b>Toxicity</b>	Human ether-a-go-go related gene (hERG) Blockers	0.044	0.044	0.068	0.011
	Human Hepatotoxicity (H-HT)	0.079	0.079	0.114	0.406
	Drug-Induced Liver Injury (DILI)	0.921	0.921	0.939	0.969
	AMES Toxicity (AMES)	0.341	0.341	0.231	0.154
	Rat Oral Acute Toxicity	0.277	0.277	0.562	0.981
	FDAMDD	0.035	0.035	0.725	0.881
	Skin Sensitization	0.183	0.183	0.748	0.17
	Carcinogenicity	0.334	0.334	0.058	0.114
	Eye Corrosion	0.003	0.003	0.003	0.003
	Eye Irritation	0.197	0.197	0.24	0.132
	Respiratory Toxicity	0.027	0.027	0.038	0.082
	Bioconcentration Factors	1.104	1.104	1.035	0.639
	<b>Environmental Toxicity</b>	Tetrahymena pyriformis 50 percent growth inhibition Concentration (IGC <sub>50</sub> )	5.011	5.011	4.868
96-hour fathead minnow 50 percent lethal concentration (LC <sub>50</sub> FM)		6.831	6.831	6.758	5.788
48-hour daphnia magna 50 percent lethal concentration (LC <sub>50</sub> DM)		6.707	6.707	6.61	5.624
NR-Androgen receptor (AR)		0.023	0.023	0.014	0.012
NR-Androgen receptor ligand-binding domain (AR-LBD)		0.25	0.25	0.193	0.58
<b>Tox21 Pathway</b>	NR-Aryl hydrocarbon receptor (AhR)	0.809	0.809	0.811	0.947
	NR-Aromatase	0.587	0.587	0.536	0.952
	NR-Estrogen receptor (ER)	0.297	0.297	0.34	0.383
	NR-Estrogen receptor ligand-binding domain (ER-LBD)	0.28	0.28	0.567	0.846

	NR-Peroxisome proliferator-activated receptor-gamma (PPAR- $\gamma$ )	0.951	0.951	0.95	0.932
	SR-Antioxidant response element (ARE)	0.382	0.382	0.317	0.848
	SR-ATPase family AAA domain-containing protein 5 (ATAD5)	0.437	0.437	0.427	0.862
	SR-Heat shock factor response element (HSE)	0.867	0.867	0.857	0.538
	SR-Mitochondrial membrane potential (MMP)	0.9	0.9	0.92	0.952
	SR-p53	0.766	0.766	0.739	0.919
<b>Toxicophore Rules</b>	Acute Toxicity Rule	0 Alerts	0 Alerts	0 Alerts	0 Alerts
	Genotoxic Carcinogenicity Rule	0 Alerts	0 Alerts	0 Alerts	0 Alerts
	NonGenotoxic Carcinogenicity Rule	0 Alerts	0 Alerts	0 Alerts	0 Alerts
	Skin Sensitization Rule	10 Alerts	10 Alerts	10 Alerts	9 Alerts
	Aquatic Toxicity Rule	2 Alerts	2 Alerts	2 Alerts	4 Alerts
	Non-Biodegradable Rule	1 Alerts	1 Alerts	1 Alerts	3 Alerts
	SureChEMBL Rule	0 Alerts	0 Alerts	0 Alerts	0 Alerts

### 3.1.2 Other Characterization

The physicochemical and medicinal chemistry properties of ligand molecules are properties satisfying and the molecules can be called potent drug candidates and need further clinical and non-clinical studies to fall under drug development pipelines. The drug-likeness properties of the ligand molecules can better be understood from the bioavailability radar. The parameters (like molecular weight, van der Waals volume, density, number of hydrogen bond acceptors, number of hydrogen bond donors, number of rotatable bonds, number of rings, number of atoms in the biggest ring, number of heteroatoms, formal charge, number of rigid atoms, flexibility, number of stereocenters, topological polar surface area, the logarithm of aqueous solubility value, logarithm of the n-octanol distribution co-efficient) were studied and represented (Table 2) (Figure 2).

**Table 2** Physicochemical & Medicinal Property of Ligands.

<b>Properties</b>	<b>Values for Silibinin (31553)</b>	<b>Values for Isosilybin (3085830)</b>	<b>Values for Silychrystin (441764)</b>	<b>Values for Silidianin (11982272)</b>
Molecular weight (MW)	482.12	482.12	482.12	482.12
Van der Waals volume	459.711	459.711	459.711	453.791
Density	1.049	1.049	1.049	1.062
No. of H-bond acceptors (nHA)	10	10	10	10
No. of H-bond donors (nHD)	5	5	6	5
No. of rotatable bonds (nRot)	4	4	4	3
No. of rings (nRing)	5	5	5	7
No. of atoms in biggest rings (MaxRing)	10	10	10	10
No. of heteroatoms (nHet)	10	10	10	10
Formal charge (fChar)	0	0	0	0
No. of rigid bonds (nRig)	29	29	28	31
Flexibility	0.138	0.138	0.143	0.097
Stereo centers	4	4	4	6
Topological Polar Surface Area (TPSA)	155.14	155.14	166.14	166.89
Log of the aqueous solubility (logS)	-4.792	-4.792	-4.774	-4.242
Log of the octanol partition coefficient (logP)	2.015	2.015	1.69	2.436
LogP at physiological pH 7.4 (logD)	2.524	2.524	2.276	1.729
Quantitative Estimate of Drug-likeness (QED)	0.374	0.374	0.325	0.373
Synthetic accessibility score (SAscore)	3.992	3.992	4.199	5.753
Fraction of sp <sup>3</sup> hybridized carbons (Fsp <sup>3</sup> )	0.24	0.24	0.24	0.36
Medicinal chemistry evolution-18 (MCE-18)	97.742	97.742	101.0	128.412
Natural product-likeness score (NPscore)	1.961	1.961	2.287	1.62
Lipinski Rule	Accepted	Accepted	Accepted	Accepted
Pfizer Rule	Accepted	Accepted	Accepted	Accepted

---

GSK Rule	Rejected	Rejected	Rejected	Rejected
Golden Triangle Rule	Accepted	Accepted	Accepted	Accepted
Pan Assay Interference Compounds (PAINS)	0 Alerts	0 Alerts	0 Alerts	0 Alerts
A La Assay to detect Reactive Molecules by Nuclear Magnetic Resonance (ALARM NMR) Rule	3 Alerts	3 Alerts	3 Alerts	3 Alerts
Borane dimethylsulfide (BMS) Rule	1 Alert	1 Alert	1 Alert	0 Alert
Chelator Rule	1 Alert	1 Alert	1 Alert	2 Alert

---



**Table 3** Molecular Docking Results.

Macromolecules	Ligands	Autodock Vina Binding affinity (kcal/mole)	Hydrogen Bonding with the Residues with the Bond Distance (in Å)	Electrostatic/Hydrophobic Interactions or $\pi$ -stacking or $\pi$ -Cation Interaction Involved
Main Protease (6LU7)	Silibinin (31553)	-7.6	45-THR [2.66], 45-THR [2.23], 143-GLY [2.14], 144-SER [2.25], 145-CYS [2.42], 145-CYS [2.53], 166-GLU [2.44], 166-GLU [2.18]	165-MET [3.59]
	Isosilybin (3085830)	-8.3	143-GLY [2.0], 144-SER [2.22], 144-SER [2.28], 145-CYS [2.46], 190-THR [2.88], 191-ALA [3.0]	165-MET [3.57], 189-GLN [3.58]
	Silychristin (441764)	-8.0	141-LEU [2.44], 143-GLY [2.06], 144-SER [2.39], 145-CYS [2.40], 191-ALA [3.0]	168-PRO [3.73], 189-GLN [3.98], 189-GLN [3.70]
	Silidianin (11982272)	-7.3	199-THR [2.09], 287-LEU [2.21]	238-ASN [3.65], 272-LEU [3.52]
Nucleocapsid Phosphoprotein (6VYO)	Silibinin (31553)	-7.4	70-GLN [2.14], 73-PRO [2.76], 75-ASN [2.35], 83-GLN [3.30], 135-THR [3.36], 164-GLY [3.20]	162-PRO [3.91]
	Isosilybin (3085830)	-7.3	69-GLY [3.24], 123-TYR [3.29], 123-TYR [3.23], 137-GLY [2.20]	68-ARG [3.84], 134-ALA [3.55]
	Silychristin (441764)	-6.9	63-ASP [2.58], 126-ASN [2.45], 129-GLY [2.63]	63-ASP [3.63]
	Silidianin (11982272)	-7.5	66-PHE [2.28], 67-PRO [3.0], 69-GLY [2.04], 70-GLN [2.05], 123-TYR [2.57], 134-ALA [2.45]	68-ARG [3.83], 68-ARG [3.64], 123-TYR [3.22], 123-TYR [4.90]
Spike Protein (7BZ5)	Silibinin (31553)	-7.1	371-SER [4.84], 343-ASN [5.32]	436-TRP [6.06, 4.86], 436-TRP [3.96], 374-PHE [6.08]
	Isosilybin (3085830)	-7.1	341-VAL [2.83], 346-ARG [2.31], 348-ALA [2.22], 399-SER [2.02]	344-ALA [3.58], 348-ALA [3.48], 452-LEU [3.35]
	Silychristin (441764)	-7.5	375-SER [3.22], 378-LYS [3.60], 380-TYR [3.32], 408-ARG [2.35]	376-THR [3.79], 407-VAL [3.50], 408-ARG [3.60], 411-ALA [3.71], 380-TYR [5.46]

---

			378-LYS [3.62]
Silidianin (11982272)	-8.2	454-ARG [3.02], 457-ARG [2.87], 457-ARG [2.62], 457-ARG [3.30], 459-SER [3.58], 467-ASP [2.55], 467-ASP [2.98], 469-SER [2.46]	473-TYR [3.93], 474-GLN [3.64]

---

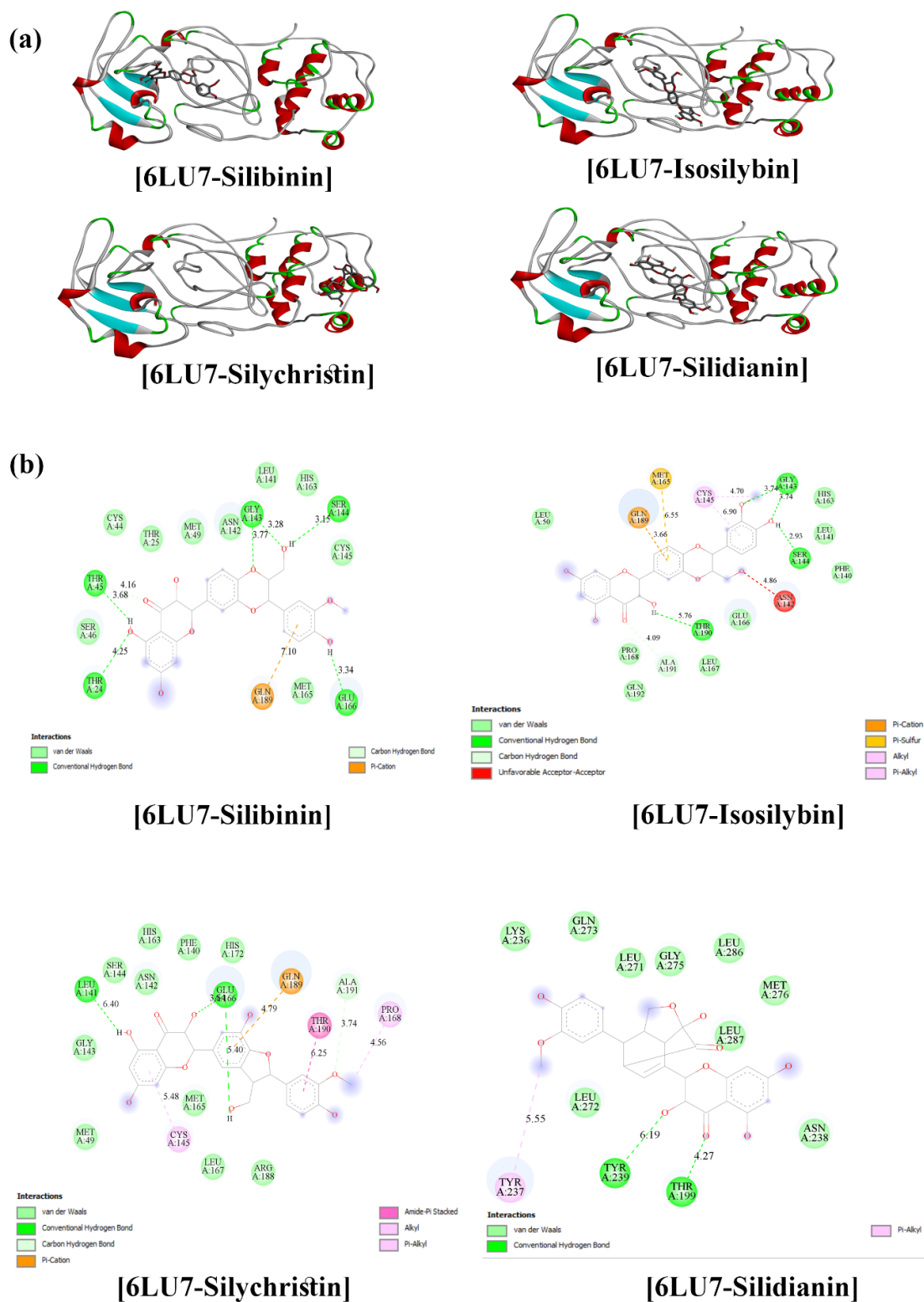


**Figure 3** Interaction of main protease (6LU7) with different ligand molecules (silibinin, isosilybin, silychristin & silidianin) in 3D diagrammatic view (a) and 2D schematic view (b).

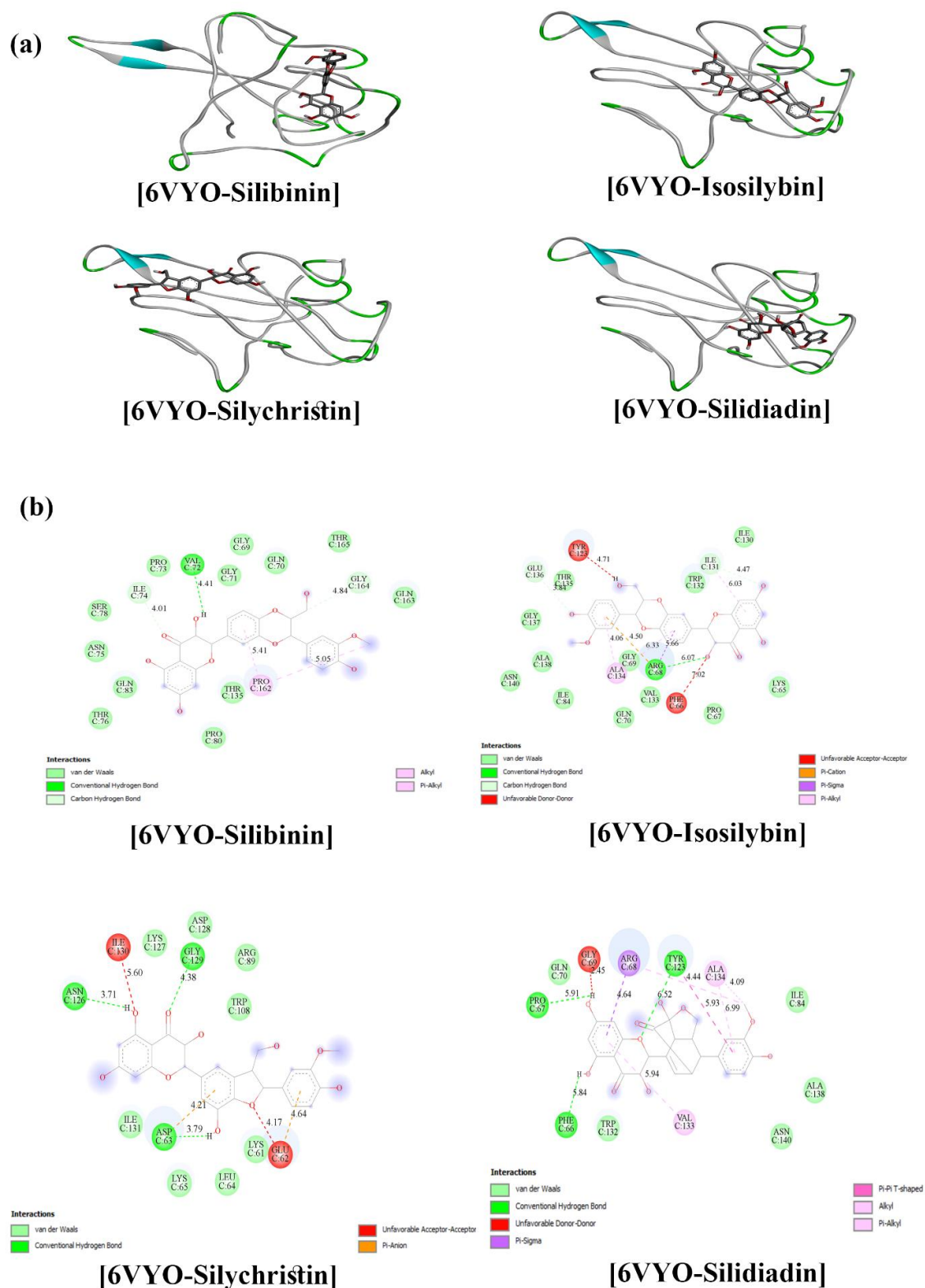


**Figure 4** Interaction of RNA binding domain of nucleocapsid phosphoprotein (6VYO) with different ligand molecules (silibinin, isosilybin, silychristin & silidianin) in 3D diagrammatic view (a) and 2D schematic. View (b).

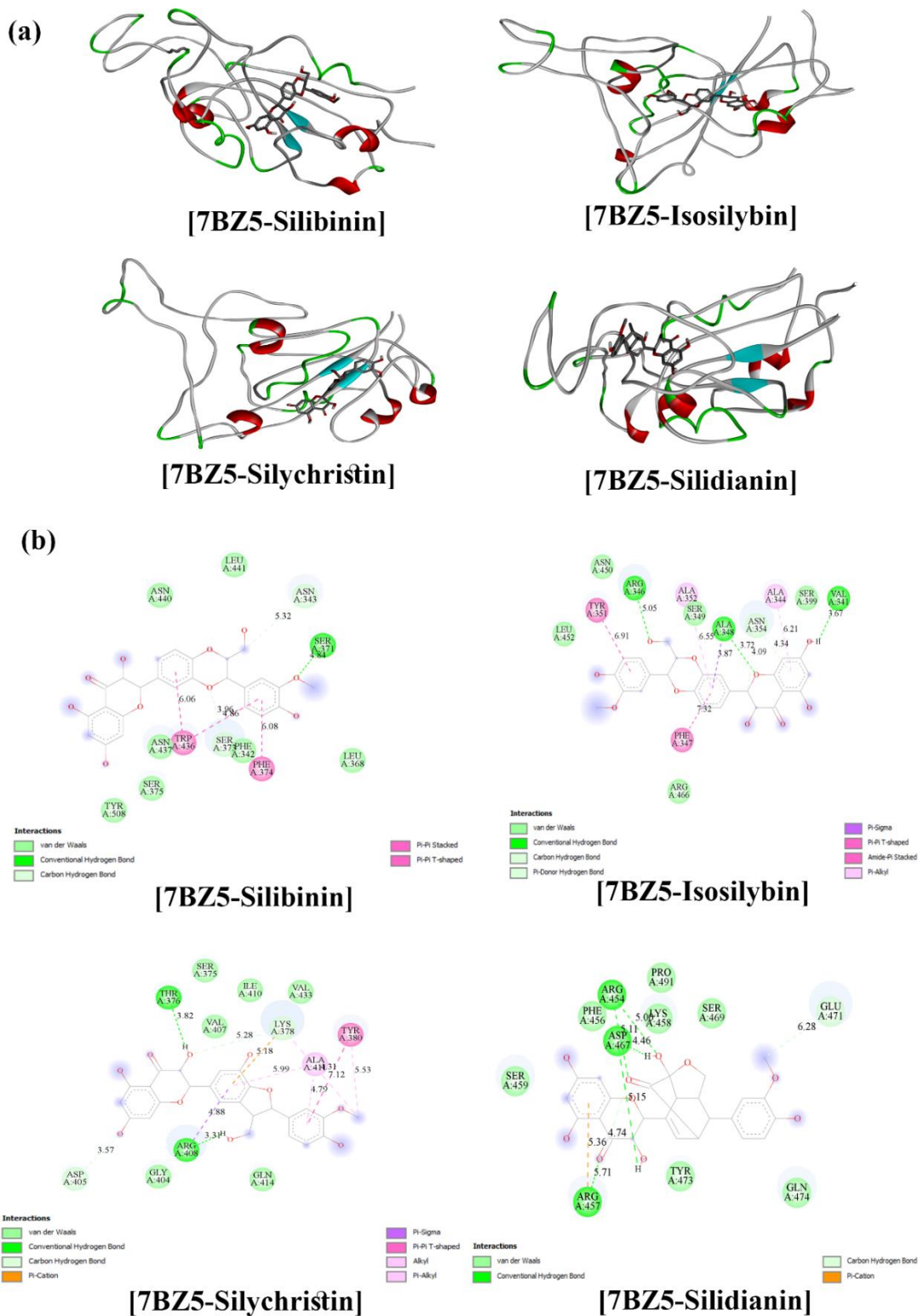


**Figure 5** Interaction of spike receptor binding domain (7BZ5) with different ligand molecules (Silibinin, isosilybin, silychristin & silidianin) in 3D diagrammatic view (a) and 2D schematic view (b).

### 3.2.2 Bioactivity Score Analysis

The four lead molecules silibinin, isosilybin, silychristin and silidianin were subjected to bioactivity score analysis based on the parameters like G protein-coupled receptors (GPCR), Ion channel modulator (ICM), Nuclear receptor ligand (NRL) and inhibitory enzymes (Protease and Kinase). The scores greater than 0.00 considered highly active; values ranging from -0.50 to 0.00 were moderately active and those less than -0.50 were inactive [25]. Based on the analysis score predicted silibinin and isosilybin were as effective due to their higher enzymatic activity inhibitor and hence can be taken forward into further drug development (Table 4).

**Table 4** Bioactivity Score of Ligands.

<b>Properties</b>	<b>Scores for Silibinin (31553)</b>	<b>Scores for Isosilybin (3085830)</b>	<b>Scores for Silychrystin (441764)</b>	<b>Scores for Silidianin (11982272)</b>
GPCR Ligand	0.07	0.07	0.25	-0.04
Ion Channel Modulator (ICM)	-0.05	-0.05	-0.12	-0.11
Kinase Inhibitor	0.01	0.01	-0.10	-0.26
Nuclear Receptor Ligand (NRL)	0.16	0.16	0.04	0.20
Protease Inhibitor	0.02	0.02	-0.06	-0.14
Enzyme Inhibitor	0.23	0.23	0.41	0.04

### 3.3 Stability of Silibinin in Protein Pockets by MD Simulations

A molecular dynamic simulation of 100 ns was analysed using the different GROMACS modules with the pre-set algorithm and the results have been explained.

#### 3.3.1 Protein Characterization

**Root Mean Square Deviation (RMSD).** The root means square deviation (RMSD) trajectory for a simulation run for three macromolecules with silibinin molecule shows the overall stability of the protein-ligand complex during the binding with active site amino acid residues of the protein molecules. The protein molecules are globular so the acceptable deviation ranges within a difference of 1-3 Å. From the C- $\alpha$  RMSD plot of the main protease (PDB ID: 6LU7) we can observe the trajectory lies within the range with very minimal deviation and after 80 ns up to 100 ns both the protein and the ligand RMSD shows a good binding affinity as in equilibrium and without any fluctuation. Likewise, if we look into the trajectory of the nucleocapsid protein (PDB ID: 6VYO) we can clearly understand that the protein molecule is very stable. The fluctuations are within 2.5 Å and most importantly during the complete 100 ns simulation, and the molecular ligand affinity shows a flattened trajectory from 78 ns up to 97 ns. And when we considered the RMSD trajectory for spike receptor binding domain (PDB ID: 7BZ5) with the ligand complex we observed the protein molecule gradually came to equilibrium in fluctuation from 68 ns up to 100 ns and surprisingly the ligand fluctuation is within 0.5 Å throughout the 100 ns simulation run (Figure 6a).

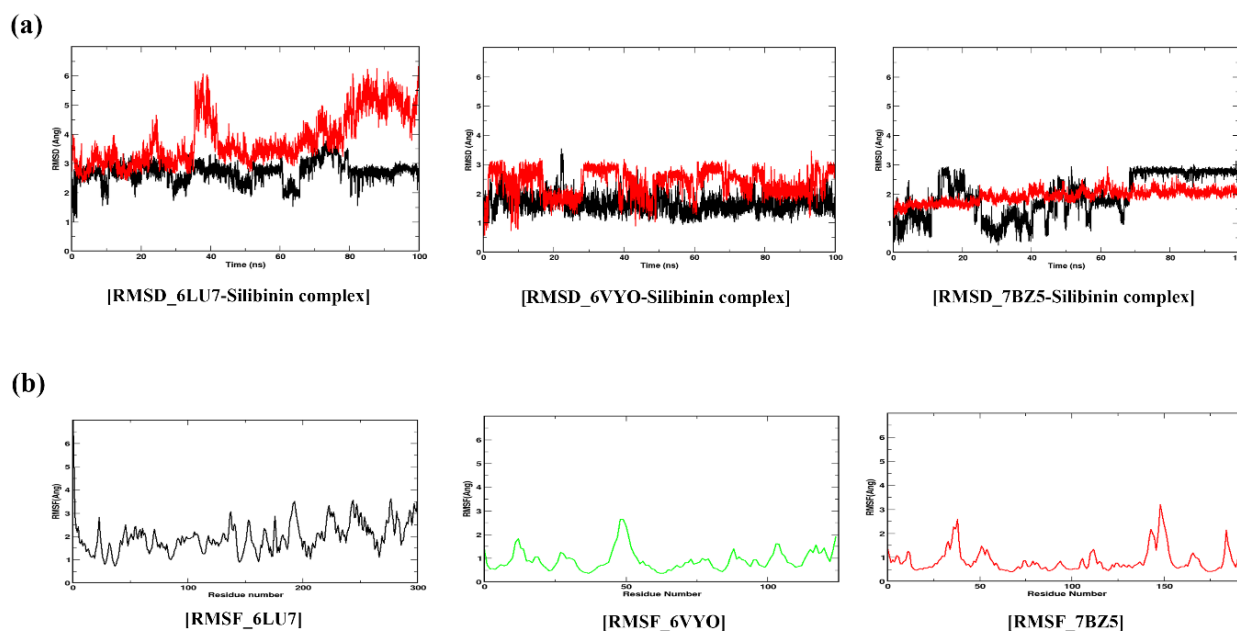


**Figure 6** (a) Root mean square deviation (RMSD) trajectories of macromolecules (6LU7, 6VYO & 7BZ5) (BLACK) with silibinin molecule (RED) and (b) Root mean square fluctuation (RMSF) trajectories of macromolecules (6LU7, 6VYO & 7BZ5) during 100 ns molecular dynamics simulation.

**Root Mean Square Fluctuation (RMSF).** The root mean square fluctuation (RMSF) of protein and ligand molecules gives the idea of each residue present in molecular structure. This calculation

generates a trajectory that denotes the flexibility of individual amino acid residues and atoms during the simulation process. When we observed the RMSF trajectory of the macromolecules we could observe the flexibility of all 306 amino acid residues of the main protease (6LU7), 128 amino acid residues of the nucleocapsid protein domain (6VYO) and 229 amino acid residues of the spike protein (7BZ5) (Figure 6b). The first 3 amino acid residues of the 6LU7 showed a high fluctuation of 6 Å. However, the fluctuation reduced to within a difference of range within 3 Å for other residues throughout the simulation run. In the case of the 6VYO protein, the fluctuation is minimal and ranges between 0.5-2.5 Å indicating no more stretching of the bonds formed between the active site residues of the complex. The trajectory of the 7BZ5 molecule also showed minimal fluctuation for a maximum number of residues during the simulation process.

Principal Component Analysis (PCA). The protein-ligand interaction results in a thousand possible poses during the simulation process and it is very difficult to analyze every pose without a statistical tool. PCA is used as a mathematical tool to detect the correlation between a large set of datasets; its biological applications are to detect the flexible regions in a protein that hinder the equilibrium state of the protein. This PCA can help integrate physical models of protein motions after removing atoms' translational and rotational movements when interacting with drug molecules. The distribution of atoms during the simulation process has been represented in the form of dot Cartesian trajectory coordinates from most eigenvector values. From our result interpretation we can predict that the interaction of drug molecules with nucleocapsid phosphoprotein and spike proteins shows very minimal changes whereas the structure of the main protease has been distorted with a large variation. The eigenvalues and eigenvectors of the covariance matrix were diagonalized with the first two principal components, i.e., PC1 & PC2 and the first 25 eigenvectors were considered (Figure 7). We conclude the silibinin drug shows maximum effectiveness against the main protease (i.e., 6LU7) and can be used as a target against the maturation of viral accessory polyproteins inside the host cells and hence be helpful for the retardation of viral proliferation [26-28]. When we observed the PCA plot for nucleocapsid phosphoprotein and spike glycoprotein we can state that residues of proteins showed less movement during the simulation process and hence preferred to remain in a natural state.

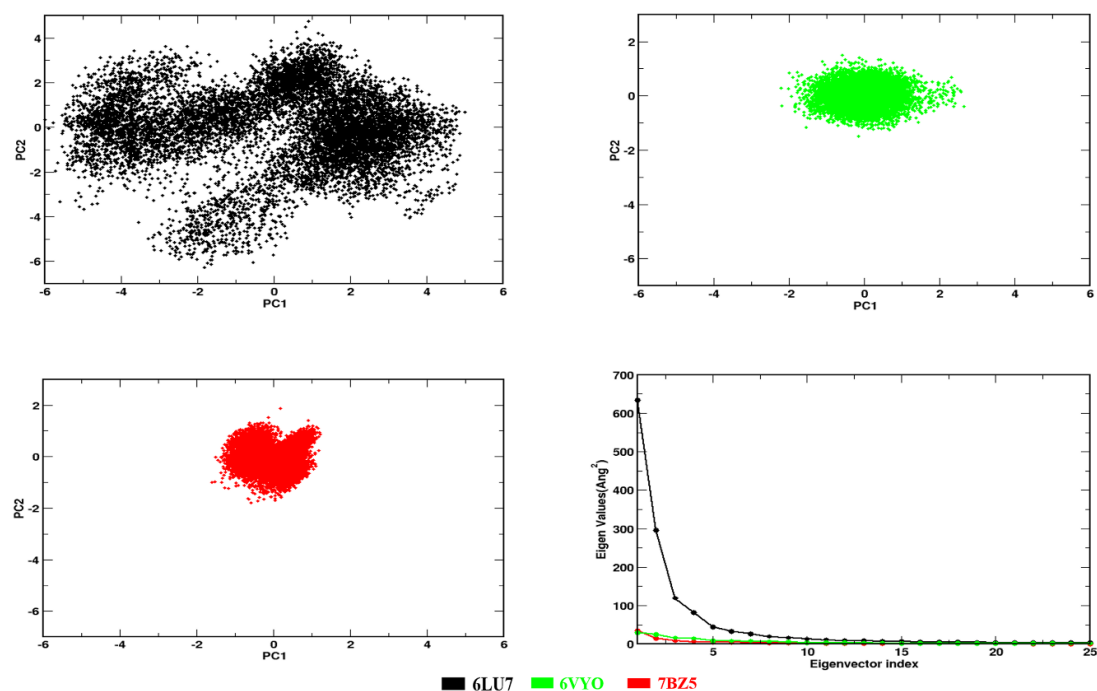


**Figure 7** PCA of different macromolecules (6LU7, 6VYO & 7BZ5) and eigen values of the covariance matrix during 100 ns simulation process.

Secondary Structure (SS). During the protein-ligand interaction, secondary structural changes occur in protein molecules along with the evolution of time using the DSSP command line tool of GROMACS. The changes in the elements like helix and beta-sheets were thoroughly observed for all the residues of the three proteins and ligand binding complexes (Figure 8). A very minute fluctuation occurred in the turns,  $\alpha$ -helix and 3-10 helix of 6LU7 (main protease). In the case of 6VYO (nucleocapsid phosphoprotein) we can visualize that the turns,  $\beta$ -sheets,  $\beta$ -turns, 3-10 helix and coils show a minimal alteration in natural structures. Similarly, if we consider the 7BZ5 (spike protein) we have observed the distortion in the second segment as compared to the natural structure in the turns,  $\alpha$ -helix,  $\pi$ -helix, 3-10 helix whereas  $\beta$ -sheets and  $\beta$ -turns show minimal fluctuations. Since the structural integrity of protein depends on the backbones of protein, a protein's secondary structure plays a vital role in protein folding and misfolding [29]. In the case of the intervention of drug molecules the distortion of protein structure occurs and protein functions and bioactivity get disturbed [30, 31]. The *in silico* interaction of the silibinin molecule with the main protease and the spike protein shows promising results in distortion of the secondary structures at different backbone residues and hence can affect the protein conformational changes leading to protein functionality [32].

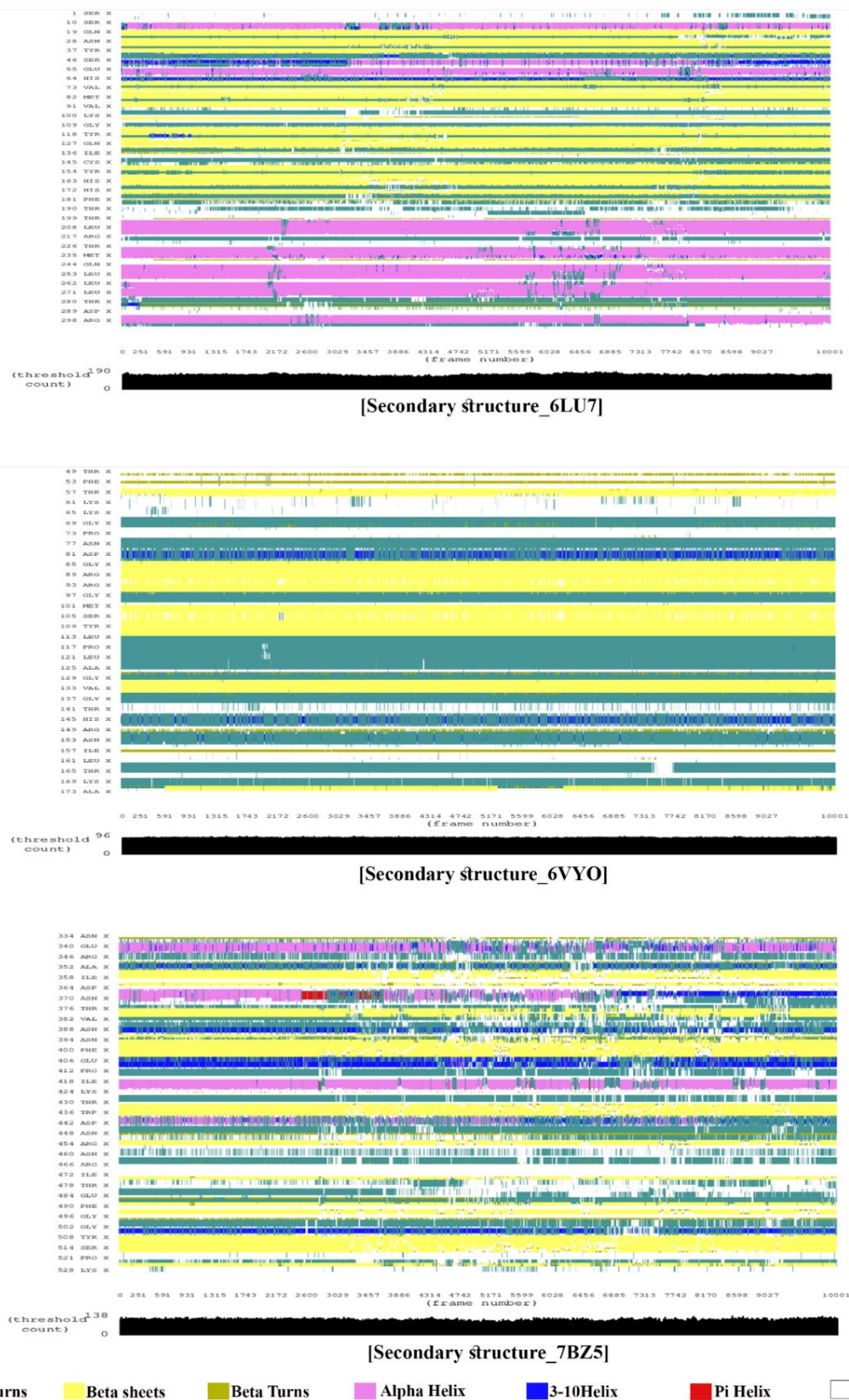


**Figure 8** Secondary structure of macromolecules (6LU7, 6VYO & 7BZ5) during 100 ns MD simulation process.

### 3.3.2 Ligand Characterization

**Root Mean Square Fluctuation (RMSF).** We have also analysed ligand flexibility of the molecules of silibinin compound during a simulation run the trajectory for all atoms and observed deviation falls within the difference of maximum 3 Å for all three different molecular binding sets and represented below (Figure 9). The more the atoms', the more the atoms' flexibility to bind with active site residues of the protein molecules leads to stronger molecular interaction among protein and ligand molecules [33]. It is being observed that all three proteins formed efficient binding interaction with silibinin molecules during the 100 ns MD simulation process and hence can be considered as a good inhibitory molecule [34].

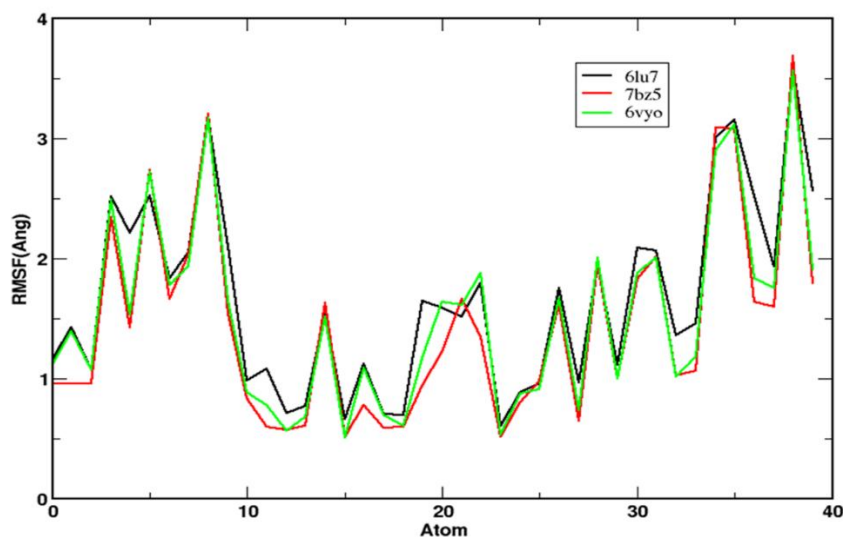


**Figure 9** RMSF of silibinin ligand with different macromolecules (6LU7, 6VYO & 7BZ5) during 100 ns MD simulation.

**Radius of Gyration (Rg).** The radius of gyration is defined as the distribution of atoms in a protein molecule around its axis. During the binding of a lead compound with protein the conformational changes in structure are observed as the compactness of the molecule gets disturbed due to different binding forces. The lesser deviations in values from the central axis during the simulation process more the structural integrity of the molecules is preserved [35]. Hence, the Rg plotted below shows much less fluctuation within a difference in the 0.5-1 Å (Figure 10a). This also predicts compactness of macromolecules is not getting disturbed when binding with silibinin inside the *in silico* environment [36].

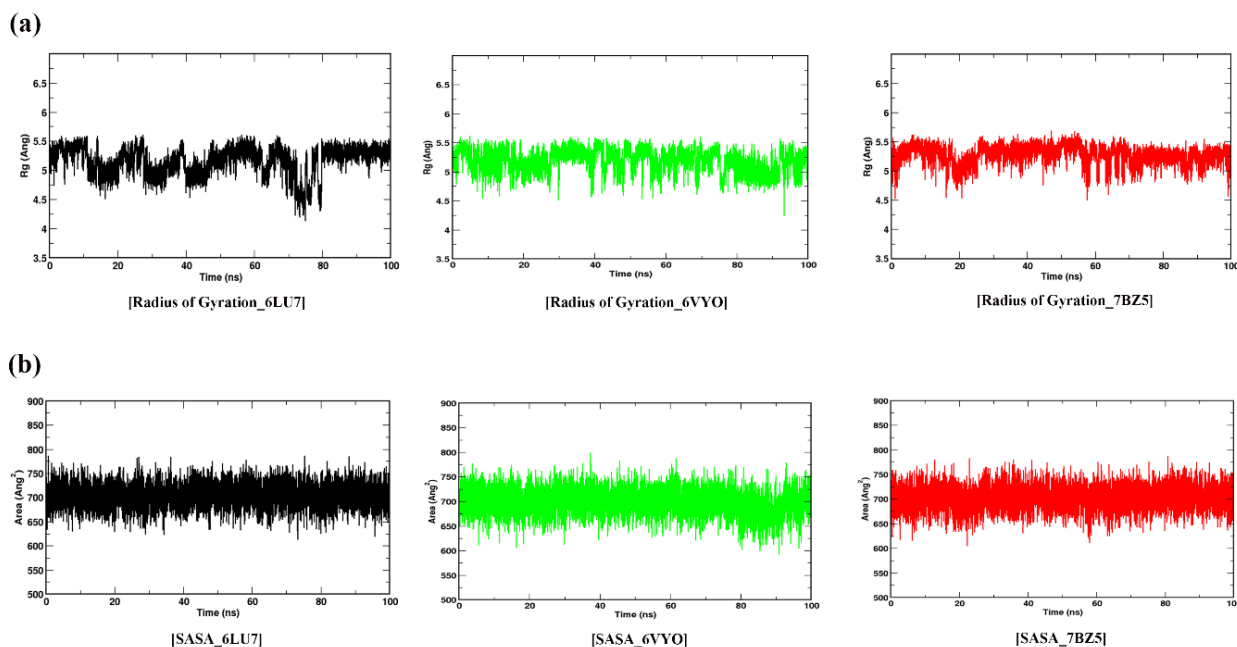


**Figure 10** Radius of Gyration (a) and solvent accessible surface area (b) of different macromolecules (6LU7, 6VYO & 7BZ5) during 100 ns MD simulation process.

Solvent Accessible Surface Area (SASA). The protein-ligand binding is a solvent-substitution process in which the protein gets unfolded to provide a surface area on the active site residues of the proteins when exposed to a solvent system. After molecular dynamics simulation, it is highly necessary to compute the SASA which shows how efficiently the computational system can mimic the intracellular physiological environment [37]. The low fluctuation in the SASA value during the simulation process suggests the very good inhibitory action of the molecule against the protein targets [38, 39]. While the binding of the molecules with the ligand molecule parts of the proteins are buried inside the solvent and few portions are exposed to the solvent; the trajectory below represents that the fluctuation of the SASA values is within a different range of 150 Å<sup>2</sup> and are the surface that is exposed into the solvent system (Figure 10b).

### 3.3.3 Protein-Ligand Interaction Profile

The molecular dynamics simulation of different proteins of SARS-CoV-2 with silibinin compounds shows good interaction during the active pocket residue of proteins with the binding site of ligand molecules (Table 5). The last frame complex during the simulation process was analyzed with the help of PLIP [24] and BIOVIA Discovery Studio Visualizer [22]. The 3D interaction of the complexes and the 2D interactions of complexes have been represented (Figure 11). We conclude that among the interaction of three macromolecules the maximum number of hydrogen bonding with bond orders less than 3.5 Å was seen between active site residues of the main protease and ligand molecule. Whereas several hydrophobic interactions have been found between ligand and spike protein, since the complete process uses water as a solvent system, we can elucidate that the hydrogen bonding is the strongest interaction and more efficient attachment of drug candidate to the target.

**Table 5** PLIP Molecular Dynamics Simulation Results.

<b>Ligand</b>	<b>Macromolecules</b>	<b>Hydrogen Bonding with the Residues with the Bond Distance (in Å)</b>	<b>Electrostatic/Hydrophobic Interactions Involved</b>	<b><math>\pi</math>-stacking or <math>\pi</math>-Cation Interaction Involved</b>
Silibinin (31553)	Main Protease (6LU7)	45-THR [1.70, 2.63], 46-SER [2.41, 3.25], 143-GLY [3.72, 4.08], 144-SER [1.73, 2.64], 166-GLU [2.53, 3.39], 189-GLN [1.95, 2.91]	165-MET [3.94]	41-HIS [4.62]
	Nucleocapsid Phosphoprotein (6VYO)	76-THR [2.67, 3.66], 77-ASN [3.09, 3.62]	52-TRP [3.45], 77-ASN [3.88], 157-ILE [3.70]	52-TRP [4.75]
	Spike Protein (7BZ5)	367-VAL [1.93, 2.82], 370-ASN [2.59, 3.36], 436-TRP [2.23, 3.19]	367-VAL [3.20], 436-TRP [3.30], 441-LEU [3.85]	509-ARG [5.51]

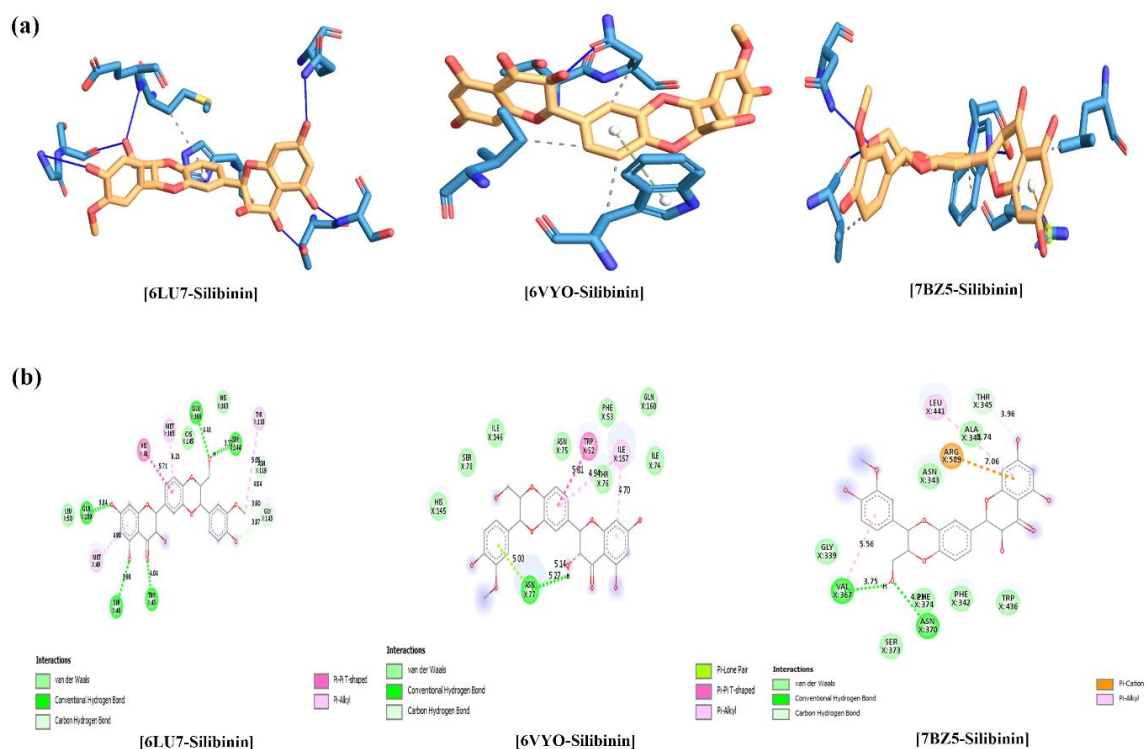


**Figure 11** Protein-ligand interaction profile (PLIP) of silibinin with different macromolecules (6LU7, 6VYO & 7BZ5) in 3D (a) & 2D (b) schematic view representing different bonds and bond length after 100 ns MD simulation last frame.

#### 4. Conclusions

It would be a great aid to repurpose this medical emergency the surge in cases due to COVID-19 worldwide researchers are striving to find an efficient drug candidate to alleviate the disease progression and treatments. These study outcomes can facilitate the silibinin molecule as a promising molecule for binding to the main protease and inhibit the formation of viral accessory assembly and replication of the SARS-CoV-2. And electrostatic interaction of the silibinin molecule with the spike protein of the virus can impede the interaction of the ACE2 receptor of the host by blocking the receptor binding domain (RBD) of the spike protein. Since COVID-19 shows critical pulmonary endothelial dysfunction by clogging atrial and venous fluid flow, the reported anti-inflammatory and anti-thrombotic properties of silibinin molecule in treating hepatic diseases will be relaxing for complications during the disease progression. The reported study on the size reduction and therapeutics intervention in animal models and its cell permeability data and the pharmacovigilance study are available as this drug has been used for many years in patients suffering from liver diseases. The candidate drug silibinin should be further tested in the COVID-19 drug repurposing pipeline and if necessary, the therapy may include other existing therapeutics based on the patient's clinical condition. We believe this silibinin is a lifesaving drug in case of COVID-19 management as a multitarget drug, without any harmful side effects and investment of huge financial cost, time and effort.

## Author Contributions

YA conceptualized the study. SM performed the ADMET, molecular docking (MD) and wrote the entire manuscript with the necessary tables and sketched figures for convenient representation. SLR set the environment and carried out the molecular dynamics simulation (MDS) by using the computational resource facility of National Institute of Technology (NIT)-Warangal. SM and SLR equally contributed in this manuscript hence share the equal authorship. SM and PS checked the language and formatting of the manuscript. YA and SM critically evaluated the manuscript.

## Funding

SM is a recipient of DRDO-SRF fellowship and PS is a recipient of DRDO-JRF fellowship. The authors have not received any special funding for this work apart from this institutional financial assistance.

## Competing Interests

Authors state no conflict of interests.

## References

1. Abenavoli L, Izzo AA, Milić N, Cicala C, Santini A, Capasso R. Milk thistle (*Silybum marianum*): A concise overview on its chemistry, pharmacological, and nutraceutical uses in liver diseases. *Phytother Res*. 2018; 32: 2202-2213.
2. Shaker E, Mahmoud H, Mnaa S. Silymarin, the antioxidant component and *Silybum marianum* extracts prevent liver damage. *Food Chem Toxicol*. 2010; 48: 803-806.
3. Wang X, Zhang Z, Wu SC. Health benefits of *Silybum marianum*: Phytochemistry, pharmacology, and applications. *J Agric Food Chem*. 2020; 68: 11644-11664.
4. Bhattacharya S. Milk thistle (*Silybum marianum* L. Gaert.) seeds in health. In: *Nuts and seeds in health and disease prevention*. Amsterdam, Netherlands: Elsevier; 2011. pp. 759-766.
5. El Mesallamy HO, Metwally NS, Soliman MS, Ahmed KA, Abdel Moaty MM. The chemopreventive effect of ginkgo biloba and *Silybum marianum* extracts on hepatocarcinogenesis in rats. *Cancer Cell Int*. 2011; 11: 38.
6. Elyasi S. *Silybum marianum*, antioxidant activity, and cancer patients. In: *Cancer*. Amsterdam, Netherlands: Elsevier; 2021. pp. 483-493.
7. Paul S, Arya A, Gangwar A, Bhargava K, Ahmad Y. Size restricted silymarin suspension evokes integrated adaptive response against acute hypoxia exposure in rat lung. *Free Radic Biol Med*. 2016; 96: 139-151.
8. Zhou H, Fang Y, Xu T, Ni WJ, Shen AZ, Meng XM. Potential therapeutic targets and promising drugs for combating SARS-CoV-2. *Br J Pharmacol*. 2020; 177: 3147-3161.
9. Ambade V, Ambade S. SARS-CoV-2 infecting endothelial cells, biochemical alterations, autopsy findings and outcomes in COVID-19, suggest role of hypoxia-inducible factor-1. *J Med Biochem*. 2022; 41: 14.
10. Mohanty S, Paul S, Ahmad Y. Understanding the SARS-CoV-2 virus to mitigate current and future pandemic (s). *VirusDisease*. 2021; 32: 390-399.

11. Luo R, Delaunay-Moisan A, Timmis K, Danchin A. SARS-CoV-2 biology and variants: Anticipation of viral evolution and what needs to be done. *Environ Microbiol.* 2021; 23: 2339-2363.
12. V'kovski P, Kratzel A, Steiner S, Stalder H, Thiel V. Coronavirus biology and replication: Implications for SARS-CoV-2. *Nat Rev Microbiol.* 2021; 19: 155-170.
13. O'Boyle NM, Banck M, James CA, Morley C, Vandermeersch T, Hutchison GR. Open babel: An open chemical toolbox. *J Cheminform.* 2011; 3: 33.
14. Trott O, Olson AJ. AutoDock Vina: Improving the speed and accuracy of docking with a new scoring function, efficient optimization, and multithreading. *J Comput Chem.* 2010; 31: 455-461.
15. Abraham MJ, Murtola T, Schulz R, Páll S, Smith JC, Hess B, et al. GROMACS: High performance molecular simulations through multi-level parallelism from laptops to supercomputers. *SoftwareX.* 2015; 1: 19-25.
16. Pronk S, Páll S, Schulz R, Larsson P, Bjelkmar P, Apostolov R, et al. GROMACS 4.5: A high-throughput and highly parallel open source molecular simulation toolkit. *Bioinformatics.* 2013; 29: 845-854.
17. Best RB, Zhu X, Shim J, Lopes PE, Mittal J, Feig M, et al. Optimization of the additive CHARMM all-atom protein force field targeting improved sampling of the backbone  $\varphi$ ,  $\psi$  and side-chain  $\chi_1$  and  $\chi_2$  dihedral angles. *J Chem Theory Comput.* 2012; 8: 3257-3273.
18. Huang J, Rauscher S, Nawrocki G, Ran T, Feig M, De Groot BL, et al. CHARMM36m: An improved force field for folded and intrinsically disordered proteins. *Nat Methods.* 2017; 14: 71-73.
19. Gutiérrez IS, Lin FY, Vanommeslaeghe K, Lemkul JA, Armacost KA, Brooks III CL, et al. Parametrization of halogen bonds in the CHARMM general force field: Improved treatment of ligand-protein interactions. *Bioorg Med Chem.* 2016; 24: 4812-4825.
20. DeLano WL. Pymol: An open-source molecular graphics tool. *CCP4 Newsl. Protein Crystallogr.* 2002; 40: 82-92.
21. Makarewicz T, Kaźmierkiewicz R. Improvements in GROMACS plugin for PyMOL including implicit solvent simulations and displaying results of PCA analysis. *J Mol Model.* 2016; 22: 109.
22. Biovia DS. BIOVIA workbook, release 2017; BIOVIA pipeline pilot, release 2017. San Diego: Dassault Systèmes; 2020.
23. Norinder U, Bergström CA. Prediction of ADMET properties. *ChemMedChem.* 2006; 1: 920-937.
24. Salentin S, Schreiber S, Haupt VJ, Adasme MF, Schroeder M. PLIP: Fully automated protein-ligand interaction profiler. *Nucleic Acids Res.* 2015; 43: W443-W447.
25. Ertl P, Rohde B, Selzer P. Fast calculation of molecular polar surface area as a sum of fragment-based contributions and its application to the prediction of drug transport properties. *J Med Chem.* 2000; 43: 3714-3717.
26. Cui W, Yang K, Yang H. Recent progress in the drug development targeting SARS-CoV-2 main protease as treatment for COVID-19. *Front Mol Biosci.* 2020; 7: 616341.
27. Huff S, Kummetha IR, Tiwari SK, Huante MB, Clark AE, Wang S, et al. Discovery and mechanism of SARS-CoV-2 main protease inhibitors. *J Med Chem.* 2021; 65: 2866-2879.
28. Ullrich S, Nitsche C. The SARS-CoV-2 main protease as drug target. *Bioorganic Med Chem Lett.* 2020; 30: 127377.
29. Alazmi M, Motwalli O. In silico virtual screening, characterization, docking and molecular dynamics studies of crucial SARS-CoV-2 proteins. *J Biomol Struct Dyn.* 2021; 39: 6761-6771.

30. Vázquez P, Hermosilla P, Guallar V, Estrada J, Vinacua À. Visual analysis of protein-ligand interactions. *Comput Graph Forum*. 2018; 37: 391-402.
31. AlAjmi MF, Azhar A, Owais M, Rashid S, Hasan S, Hussain A, et al. Antiviral potential of some novel structural analogs of standard drugs repurposed for the treatment of COVID-19. *J Biomol Struct Dyn*. 2021; 39: 6676-6688.
32. Ahamad S, Kanipakam H, Gupta D. Insights into the structural and dynamical changes of spike glycoprotein mutations associated with SARS-CoV-2 host receptor binding. *J Biomol Struct Dyn*. 2022; 40: 263-275.
33. Avti P, Chauhan A, Shekhar N, Prajapat M, Sarma P, Kaur H, et al. Computational basis of SARS-CoV2 main protease inhibition: An insight from molecular dynamics simulation based findings. *J Biomol Struct Dyn*. 2021; 40: 8894-8904.
34. Mishra D, Maurya RR, Kumar K, Munjal NS, Bahadur V, Sharma S, et al. Structurally modified compounds of hydroxychloroquine, remdesivir and tetrahydrocannabinol against main protease of SARS-CoV-2, a possible hope for COVID-19: Docking and molecular dynamics simulation studies. *J Mol Liq*. 2021; 335: 116185.
35. Peele KA, Durthi CP, Srihansa T, Krupanidhi S, Ayyagari VS, Babu DJ, et al. Molecular docking and dynamic simulations for antiviral compounds against SARS-CoV-2: A computational study. *Inform Med Unlocked*. 2020; 19: 100345.
36. Parida PK, Paul D, Chakravorty D. The natural way forward: Molecular dynamics simulation analysis of phytochemicals from Indian medicinal plants as potential inhibitors of SARS-CoV-2 targets. *Phytother Res*. 2020; 34: 3420-3433.
37. Kumar S, Sharma PP, Shankar U, Kumar D, Joshi SK, Pena L, et al. Discovery of new hydroxyethylamine analogs against 3CLpro protein target of SARS-CoV-2: Molecular docking, molecular dynamics simulation, and structure–activity relationship studies. *J Chem Inf Model*. 2020; 60: 5754-5770.
38. Rahman MM, Saha T, Islam KJ, Suman RH, Biswas S, Rahat EU, et al. Virtual screening, molecular dynamics and structure–activity relationship studies to identify potent approved drugs for COVID-19 treatment. *J Biomol Struct Dyn*. 2021; 39: 6231-6241.
39. Rafi MO, Bhattacharje G, Al-Khafaji K, Taskin-Tok T, Alfasane MA, Das AK, et al. Combination of QSAR, molecular docking, molecular dynamic simulation and MM-PBSA: Analogues of lopinavir and favipiravir as potential drug candidates against COVID-19. *J Biomol Struct Dyn*. 2020; 40: 3711-3730.